2005

Airborne Measurements of Areal Spectral Surface Albedo over Different Sea and Land Surfaces

Wendisch, Manfred

Airborne measurements of areal spectral surface albedo over different sea and land surfaces

Manfred Wendisch,[1,2] Peter Pilewskie,[2] Evelyn Jäkel,[1] Sebastian Schmidt,[1] John Pommier,[3] Steve Howard,[3] Haflidi H. Jonsson,[4] Hong Guan,[3] Marc Schröder,[5] and Bernhard Mayer[6]

Received 26 November 2003; revised 12 February 2004; accepted 4 March 2004; published 17 April 2004.

[1] Airborne measurements of the ratio of spectral upward and downward irradiances (so-called spectral albedo) are used to derive the areal spectral surface albedo in the wavelength range from 330 to 1670 nm. The data were collected over different sea and land surfaces in cloudless atmospheric conditions during three field campaigns. Measurements from the Albedometer (developed at IfT) and the NASA Solar Spectral Flux Radiometer (SSFR) are employed. Spectral radiative transfer calculations show that atmospheric scattering and absorption within the layer beneath the flight level considerably contribute to the airborne albedo measurements reported here, even for low flight altitudes (0.2–0.5 km). To remove this atmospheric masking, a nonlinear extrapolation of the airborne albedo measurements to the ground is performed. The nonlinearity is due to the vertically inhomogeneous distribution of the particle microphysical properties. This fact underlines the importance of aerosol profile measurements for the proper correction of atmospheric masking. Examples of the extrapolated areal spectral surface albedos are discussed in terms of their solar zenith angle dependence, their small-scale, and general variability. Finally, typical areal spectral surface albedos for different sea and land surfaces, as derived from the three measurement campaigns, are supplied in parameterized form for use in radiative transfer applications. *INDEX TERMS:* 0305 Atmospheric Composition and Structure: Aerosols and particles (0345, 4801); 1694 Global Change: Instruments and techniques; 3359 Meteorology and Atmospheric Dynamics: Radiative processes; 3360 Meteorology and Atmospheric Dynamics: Remote sensing; *KEYWORDS:* areal spectral surface albedo, spectral radiative transfer, aerosol particles

Citation: Wendisch, M., P. Pilewskie, E. Jäkel, S. Schmidt, J. Pommier, S. Howard, H. H. Jonsson, H. Guan, M. Schröder, and B. Mayer (2004), Airborne measurements of areal spectral surface albedo over different sea and land surfaces, *J. Geophys. Res.*, *109*, D08203, doi:10.1029/2003JD004392.

1. Introduction

[2] The surface albedo is an important boundary condition for atmospheric solar radiative transfer models. It is defined as the ratio of diffuse upward and global (i.e., direct plus diffuse) downward solar irradiances at the Earth's surface. The solar energy reflected by the surface is available for further radiative interactions (scattering/absorption on air molecules and aerosol/cloud particles) within the atmosphere. The complementary part of the incident solar energy, which is not reflected from the ground back to the atmosphere, is absorbed by the surface. It heats the ground and is transformed into long-wave radiation and then reemitted by the Earth's surface. In this way the surface albedo is important (1) for multiple scattering and absorption processes in the solar spectral range within the atmosphere, and (2) for the transformation of radiation energy from the solar to the terrestrial wavelength range at the ground. Thus the surface albedo is a constraining factor for the surface and atmosphere energy budgets.

[3] In general the term albedo is defined as a ratio of upward and downward irradiances for any altitude. At the ground the albedo is identical with the surface albedo. At all other altitudes the albedo includes contributions due to reflections originating from the surface, as well as influences due to reflection and multiple scattering within the atmosphere above and beneath the considered height (so-called atmospheric masking). Therefore sometimes the albedo is called the effective albedo [e.g., *Webb et al.*, 2000]. In this paper this term is omitted.

[1]Leibniz-Institute for Tropospheric Research (IfT), Leipzig, Germany.
[2]Earth Science Division, National Aeronautics and Space Administration (NASA), Ames Research Center (ARC), Moffett Field, California, USA.
[3]Bay Area Environmental Research (BAER) Institute, Sonoma, California, USA.
[4]Center for Interdisciplinary Remotely-Piloted Aircraft Studies (CIRPAS), Marina, California, USA.
[5]Institute for Space Sciences, Free University of Berlin (FUB), Berlin, Germany.
[6]Institute of Atmospheric Physics, Deutsches Zentrum für Luft- und Raumfahrt (DLR), Oberpfaffenhofen, Germany.

0148-0227/04/2003JD004392$09.00

[4] *Kiehl and Trenberth* [1997] give a globally and annually averaged value of the broadband-solar (i.e., averaged over the solar wavelength range) surface albedo of about 0.18. However, such a value is of limited use for specific applications, because the surface albedo varies considerably for different ground types. Over sea the surface albedo is generally much less than 0.18, over land it is larger for most parts of the solar spectrum. In addition the surface albedo over land is more variable because it is a function of soil/vegetation type and the season of the year. Even if these influences are accounted, broadband-solar surface albedo values are not sufficient for the interpretation of broadband-solar radiation applications [*Michalsky et al.*, 2003], and in particular for the interpretation of spectral radiation data.

[5] Therefore several authors have studied the spectral surface albedo for different types of reflecting ground and wavelength ranges. Mostly measurements are reported which are directly obtained at the surface [e.g., *Coulson and Reynolds*, 1971; *Bowker et al.*, 1985; *Blumthaler and Ambach*, 1988; *Feister and Grewe*, 1995; *Aoki et al.*, 2002]. However, to interpret aircraft measurements with the help of one-dimensional radiative transfer models, these ground-based measurements may not be appropriate, because the aircraft flies over inhomogeneous terrain receiving a mixed reflection signal from several types of surfaces. For this purpose the so-called areal-averaged or shorter the areal surface albedo has to be determined. This quantity includes the reflection properties of the underlying inhomogeneous surface and is best suited to interpret airborne radiation measurements.

[6] Airborne measurements of spectral albedo at certain flight altitudes are presented by *Webb et al.* [2000] for the wavelength range from 290 to 500 nm. These airborne albedo data are not corrected for atmospheric masking. In a subsequent study, A. R. Webb et al. (Airborne measurements of ground and cloud spectral albedos under low aerosol loads, submitted to *Journal of Geophysical Research*, 2004) perform a linear extrapolation of their airborne albedo measurements to the ground. In the present paper this work is continued by extending the wavelength range of the measurements to 330–1670 nm and by applying a nonlinear surface extrapolation method to retrieve the areal spectral surface albedo from airborne spectral albedo measurements.

[7] *Li et al.* [2002] derive areal spectral surface albedo (cloudy conditions) from a method combining ground-based downward solar transmittance measurements and radiative transfer calculations. With this approach the authors achieve a significantly improved match between measured and calculated solar spectral transmittance, especially in the near-infrared spectral region. This study by *Li et al.* [2002] clearly demonstrates that, even in cloudy conditions, areal spectral surface albedo is a crucial function to correctly describe solar radiative transfer due to significance of multiple scattering.

[8] In section 2 of this paper the modeling and experimental tools used here are introduced. The measurements are collected in cloudless conditions in three field campaigns, which are briefly described at the end of section 2. In section 3 simulated and measured profiles of the spectral albedo over sea and land are analyzed for two specific cases. It is shown that, in order to retrieve the areal spectral surface albedo from the albedo measurements at a certain flight level, a nonlinear surface extrapolation technique is required, which is introduced in section 4. In section 5 the nonlinear surface extrapolation method is applied to data collected during the field campaigns. The results are discussed in terms of their solar zenith angle dependence, their small-scale variability and variation for different terrains. A summary of the paper is given and respective conclusions are drawn in section 6.

2. Methods and Material

[9] In this paper radiative transfer modeling is combined with airborne meteorological, aerosol microphysical, and radiation measurements to retrieve areal spectral surface albedo for different sea and land surfaces. The components of this approach are introduced in the following two subsections. In the third subsection 2.3 two specific measurement cases are briefly introduced.

2.1. Spectral Radiative Transfer Model

[10] A one-dimensional (vertical) radiative transfer model is applied which calculates both spectral and broadband (solar and terrestrial) global downward and diffuse upward irradiances or radiances as a function of altitude above ground. The approach is based on the 'Matrix Operator Method'. The radiative transfer equation is solved for a vertically inhomogeneous atmosphere by a combination of the 'Discrete Ordinate Method' for each homogeneous sublayer and the 'Adding Method' for linking the sublayers [*Nakajima and Tanaka*, 1986, 1988]. The zenith angle (upper atmospheric hemisphere) is divided into eight streams by a Gaussian quadrature scheme. Beside multiple scattering, the model accounts for gaseous absorption using the gas absorption coefficients adopted from LOWTRAN-7 [*Kneizys et al.*, 1988]. No actual measurements of ozone concentrations were used. Instead climatological data are applied which are defined by the standard atmosphere used in the radiative transfer calculations. The vertical resolution of the model is fixed to 20 m below 5 km altitude and to 1 km from 5 to 12 km altitude. Additional altitudes are 20, 40, and 100 km. In total, 260 atmospheric layers are considered. Further details of the model are described elsewhere [e.g., *Wendisch et al.*, 2002].

[11] The model has participated in the Inter Comparison of Radiation Codes in Climate Models, Phase III (ICRCCM-III) project [*Barker et al.*, 2003] and proven its good shape in this exercise. If not stated otherwise spectral surface reflectance data by *Bowker et al.* [1985] are used as the lower boundary condition to describe the spectral surface albedo. The extraterrestrial spectral irradiances at the top of the atmosphere are adapted from LOWTRAN-7. These upper boundary condition data are adjusted to the actual Earth-Sun distance. The solar zenith angle is calculated using date, local time and geographical information. As a key input the model requires profile measurements of meteorological (air temperature, relative humidity, air pressure) and particle (aerosol, water droplets, or ice) microphysical parameters (number concentration, effective radius, standard deviation of the lognormal fit of the respective size distribution), including their humidity dependence. Above the highest measurement altitudes the meteorological and microphysical model input profiles are completed by stan-

Table 1. Brief Summary of the Three Measurement Campaigns Included in This Study

	NORTH-SEA-2000	BBC-2001	CRYSTAL-FACE-2002
Scientific Focus	Cloudless Sky	Boundary Layer Clouds	Cirrus Clouds
Time Period	September 2000	September 2001	July 2002
Campaign Area	Germany	The Netherlands	USA
	(North Sea Coast)	(Around Cabauw)	(Southern Florida)
	≈54.3°N, 9.5°E	≈51.6°N, 4.6°E	≈24.6°N, 81.7°W
Aircraft	Partenavia P68B	Partenavia P68B	Twin Otter UV-18A
Radiometer	Albedometer	Albedometer	Solar Spectral Flux Radiometer (SSFR)
Reference	*Wendisch and Mayer* [2003]	*Crewell et al.* [2004]	*Jensen et al.* [2004]

dard assumptions (meteorological profiles by *Anderson et al.* [1986] and aerosol profiles by *Shettle* [1989]). Up to eight modes for the particle size distributions can be combined in the radiative transfer model, and different values of spectral refractive indices (as function of relative humidity) can be assigned to each of them. In this way numerous internal and external aerosol mixtures can be investigated. For the cases in subsection 2.3, mixtures of ammonium sulfate and soot have been assumed as described by *Wendisch and Mayer* [2003]; otherwise the spectral refractive indices of ammonium sulfate have been applied in the radiative transfer calculations.

2.2. Field Campaigns and Instrumentation

[12] Data from three field campaigns with different scientific objectives are used in this study. In spite of these differences, all three campaigns require the areal spectral surface albedo as one of the key input parameters for the radiative transfer models used to analyze the field data. The campaigns are briefly introduced in Table 1. The NORTH-SEA-2000 experiment investigated the influence of aerosol particles on the spectral radiative properties of a cloudless atmosphere. It took place at the North Sea coast in Germany in September 2000. Spatial and temporal inhomogeneities of boundary layer clouds and their influence on atmospheric radiative transfer were studied during Baltex Bridge Campaign (BBC-2001), which was conducted in the Netherlands (near Cabauw) in September 2001. In the NORTH-SEA-2000 and the BBC-2001 experiments several aircraft were operated, here data are reported which were obtained from an aircraft of the type Partenavia P68B. In 2002 the Cirrus Regional Study of Tropical Anvils and Cirrus Layers - Florida Area Cirrus Experiment (CRYSTAL-FACE-2002) was performed to analyze the microphysical and dynamical properties of cirrus anvil clouds. The measurements during CRYSTAL-FACE-2002 were achieved in southern Florida in July 2002. Among others a Twin Otter UV-18A aircraft was used in this experiment; data obtained with this aircraft are presented here.

[13] On the Partenavia the meteorological data were collected with common instrumentation [*Keil et al.*, 2001]. For the aerosol particle size distribution measurements a commercial Passive Cavity Aerosol Spectrometer Probe (PCASP-X, manufactured by Particle Measuring Systems, Inc., Boulder, CO, USA) was employed. From the particle size distributions the effective particle radius R_{eff} and particle number concentration N_p are derived. Details of the calibration and data processing can be found in *Keil et al.* [2001]. During CRYSTAL-FACE-2002 the meteorological data were obtained from drop sonde measurements while the aerosol particle microphysical parameters are derived from measurements with a PCASP-100X.

[14] The spectral radiation measurements were accomplished using two unique instruments: the Albedometer (developed at IfT) and the NASA Solar Spectral Flux Radiometer (SSFR). The Albedometer was installed on the Partenavia during the NORTH-SEA-2000 and BBC-2001 campaigns. It measures global downward and diffuse upward irradiances in a spectral range from 290 to 1000 nm (Full Width at Half Maximum, FWHM $\approx 2-3$ nm). Here Albedometer measurements in the spectral range from 330 to 995 nm are reported. For the studies in this publication, the integration time was set to 0.3 s. The Albedometer is equipped with a horizontal stabilization mechanism, which keeps the upward and downward facing sensor heads (optical collectors, also called optical inlets) in a horizontal position during the flight. The stabilization and the technical specifications of the Albedometer are described in detail by *Wendisch et al.* [2001], *Wendisch and Mayer* [2003], and *Wendisch* [2003]. An overall uncertainty for the spectral irradiance measurements with the Albedometer of ±4% for wavelengths $\lambda = 400-770$ nm and of ±6% for $\lambda \leq 400$ nm and $\lambda \geq 770$ nm is estimated [*Wendisch and Mayer*, 2003; *Wendisch*, 2003]. The cosine response of the optical inlet heads was quantified in the laboratory as a function of incident angle and wavelength. These measurements were used in the data analysis software to correct for the nonideal cosine response of the Albedometer as described by *Wendisch et al.* [2002] and in more detail by *Wendisch* [2003]. Just recently the Albedometer was modified to measure spectral actinic flux densities in addition to the spectral irradiances (E. Jäkel et al., A new airborne system for fast measurements of upwelling and downwelling spectral actinic flux densities, submitted to *Applied Optics*, 2003).

[15] The SSFR is very similar compared to the Albedometer. It also measures global downward and diffuse upward spectral irradiances, however, it covers a broader wavelength range (300 nm to 1700 nm with a FWHM of $\approx 9-12$ nm). In this paper, SSFR data for the wavelength range between 350 nm and 1670 nm with a temporal resolution of 1 s are presented. The SSFR was installed on the Twin Otter during the CRYSTAL-FACE-2002 experiment. The instrument is described by *Pilewskie et al.* [2003], along with a description of the calibration procedures, which are applied to the Albedometer in a similar manner. The overall measurement uncertainty for the spectral irradiances measured with the SSFR is identical to the measurement error of the Albedometer.

[16] For the Partenavia flights horizontal and vertical profile data are shown. However, in reality the profile measurements are smooth aircraft descents with pitch and roll angles of the aircraft of less than ±6° (the limitation of the horizontal stabilization technique of the Albedometer). Therefore the profile measurements with the Partenavia

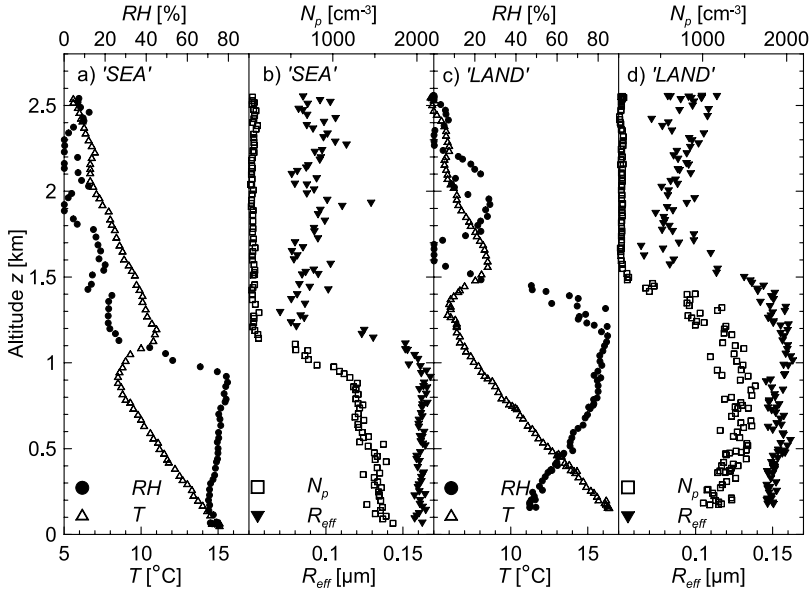

Figure 1. Profiles of meteorological (static air temperature *T*, relative humidity *RH*, Figures 1a, 1c) and aerosol particle microphysical (effective radius R_{eff}, number concentration N_p, Figures 1b, 1d) measurements. The data are taken with a 1 Hz time resolution, only each 10th measured data point is plotted. Figures 1a, 1b depict data collected over sea (case '*SEA*'), Figures 1c, 1d show measurements taken over land (case '*LAND*'). The data stem from the NORTH-SEA-2000 campaign (September 23, 2000).

reported here do not refer to strict vertical patterns and actually cover larger horizontal distances. From the Twin Otter flights only data from horizontal flight patterns are shown in this paper. The SSFR on the Twin Otter was not mounted on a stabilized platform during CRYSTAL-FACE-2002. Instead, the SSFR data used for this study was filtered to remove those irradiance values collected when the cosine of solar zenith angle with respect to the aircraft differed by more than 1% from cosine of solar zenith angle with respect to the Earth-fixed coordinate system.

2.3. Investigated Cases

[17] Two measurement cases are introduced in particular because they are widely used throughout the paper. These two cases stem from measurements during the NORTH-SEA-2000 campaign on September 23, 2000. Horizontal and vertical flight patterns over sea and land surface were conducted on that day, which makes it perfectly suited for comparison between the two different types of reflecting surfaces. These two examples are referred to as cases '*SEA*' and '*LAND*' in the subsequent text.

[18] For the radiative transfer calculations meteorological and aerosol particle microphysical profile data are needed, which are depicted in Figure 1 for the two specific cases '*SEA*' and '*LAND*'. These data are explicitly discussed here because they are a crucial input for the radiative transfer calculations. In particular, the importance of the aerosol microphysical characteristics on the areal surface albedo retrieval will be demonstrated in subsections 3.1 and 4.2. The profile data also serve as a general meteorological characterization of the two measurement cases.

[19] Figure 1a shows the meteorological measurements (static air temperature *T*, relative humidity *RH*) for the case '*SEA*'. A distinct temperature inversion in the layer between about 0.9 km and 1.2 km altitude is obvious (open triangles, lower axis), which influences the profile of *RH* (solid circles, upper axis). The nearly constant values of *RH* below the temperature inversion indicate a rather low level of mixture within the boundary layer. The microphysical parameters for the case '*SEA*' are plotted in Figure 1b. The vertical pattern of the temperature inversion is obvious in these aerosol profiles. There are rather constant values of the effective particle radius R_{eff} (solid triangles, lower axis) around 0.16–0.17 µm below the temperature inversion layer, which drop to values mostly below 0.10 µm above it. The particle concentration N_p (open squares, upper axis) decreases from 1300 to 1600 cm^{-3} in the boundary layer to values below 100 cm^{-3} above the temperature inversion layer.

[20] The corresponding data for the case '*LAND*' (Figures 1c and 1d) have been taken just after the measurements over sea. Thus the general features for the case '*LAND*' are similar to the data collected over sea. However, the temperature profile indicates that the inversion layer is slightly higher over land (1.3–1.6 km). The profile of *RH* is not constant below the temperature inversion layer which is an indication for a well-mixed boundary layer. This fact is also visible in the aerosol microphysical parameter profiles, which exhibit stronger fluctuations in the more turbulent boundary layer over land. The average values of R_{eff} and N_p below the temperature inversion are in the same range as the data collected over sea.

[21] The aerosol microphysical data indicate a relatively high aerosol burden on that specific measurement day (September 23, 2000) for both cases '*SEA*' and '*LAND*'. An aerosol optical thickness of 0.4–0.5 at 550 nm wavelength was obtained from the radiative transfer calculations

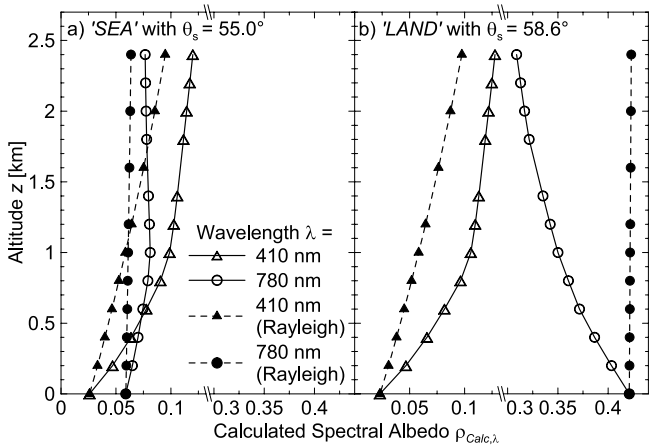

Figure 2. CALCULATED spectral albedo $\rho_{Calc,\lambda}$ (ratio of upward and downward calculated irradiances $F_{Calc,\lambda}\uparrow$ and $F_{Calc,\lambda}\downarrow$) as a function of altitude z for the two exemplarily wavelengths λ = 410 nm and λ = 780 nm. θ_s represents the solar zenith angle. Figure 2a depicts the case '*SEA*', Figure 2b shows results obtained for the case '*LAND*'.

on the basis of the microphysical measurements. No independent Sun photometer measurements were available.

3. Profiles of Spectral Albedo

3.1. Results of Calculations

[22] The meteorological and aerosol microphysical measurements presented in subsection 2.3 are used as input for radiative transfer simulations for the two measurement cases '*SEA*' and '*LAND*'. From the ratio of spectral upward and downward irradiances the spectral albedo as a function of altitude is calculated. Surface albedo (strictly these are reflectance data) data by *Bowker et al.* [1985] are utilized as lower boundary condition (type 'water' [no. 149] for the case '*SEA*' and type 'grass' [no. 73] for the case '*LAND*'). The objective is to quantify the altitude-dependence of the spectral albedo and to investigate the importance of the aerosol microphysical data on the spectral albedo.

[23] Figure 2 shows the calculated profiles of spectral albedo $\rho_{Calc,\lambda}$ for two selected wavelengths (410 nm, open and solid triangles; 780 nm, open and solid circles). Both wavelengths are not seriously affected by gas absorption. The open symbols (solid lines) represent the results including aerosol particles and gas molecules, whereas the solid symbols (dashed lines) show the spectral albedo profiles considering gas molecules only (Rayleigh atmosphere).

[24] For the case '*SEA*' (Figure 2a) and the wavelength λ = 410 nm (open triangles) the spectral albedo increases with increasing altitude. Below the temperature inversion the rate of increase is larger compared to above the inversion. This nonlinear behavior below the temperature inversion is caused by the aerosol particles, which is shown by comparison with results neglecting aerosol particles (solid triangles, Rayleigh). The increase of the spectral albedo with increasing altitude in a Rayleigh atmosphere without particle scattering is nearly linear. The profiles of spectral albedo become less steep with increasing wavelength (see the curve for λ = 780 nm as example, open circles), and so do the respective profiles for the Rayleigh atmosphere (solid circles). For 780 nm wavelength the profile of spectral albedo in a Rayleigh atmosphere is nearly height-independent. This is not surprising, because the Rayleigh optical thickness is very low for wavelengths larger than 700 nm (vertically integrated optical thickness is less than 0.04). The Rayleigh atmosphere does not mask the spectral surface albedo for larger wavelengths.

[25] For the measurement case '*LAND*' (Figure 2b) the nonlinear behavior of the spectral albedo at 410 nm (open triangles) wavelength is similar to the case '*SEA*'. Also the nearly linear vertical pattern of the spectral albedo profile for a Rayleigh atmosphere (solid triangles) is confirmed. However, the continuous decrease of the slope of the albedo profile with increasing wavelength is only observed for wavelengths less than about 700 nm. Above this wavelength (the so-called vegetation step) the spectral albedo decreases with increasing altitude (open circles). This is a qualitative difference compared to the results obtained for the case '*SEA*'. The respective Rayleigh atmosphere shows nearly height-independent spectral albedo profiles for wavelengths larger than about 700 nm (solid circles).

[26] The decrease of albedo with increasing altitude for the 780 nm profile (open circles) over land in Figure 2b can only be explained by particle absorption (gas absorption can be neglected at this wavelength). Over sea, the surface contribution to the diffuse upward irradiance is so small that the albedo generally increases with altitude (as in a nonabsorbing atmosphere), due to backscattering by aerosol particles. Over land, however, the main contribution to the diffuse upward irradiance stems from the surface and is attenuated by absorbing particles between the surface and the measurement instrument. In this case, the reduction of the surface reflected irradiance is not compensated by particle backscattering. As a proof, additional simulations of the albedo profile have been performed (not shown), assuming different values for the particle single scattering albedos. For purely scattering particles the albedo increases with increasing altitude, and this is what is to be expected because the scattering aerosol increases the diffuse upward irradiance at any altitude always more than the downward component. Only if the aerosol is absorbing the albedo may decrease with increasing altitude for 780 nm wavelength over land.

[27] In this way aerosol particles complicate the retrieval of the areal spectral surface albedo from airborne albedo measurements significantly. For a pure gas atmosphere the spectral albedo at a certain altitude could easily be extrapolated to the surface by nearly linear relationships. For larger wavelengths almost no atmospheric correction has to be performed in a Rayleigh atmosphere. When aerosol particles are present, the profile of the spectral albedo is nonlinear. In the cases presented here no simple parametrization for the surface extrapolation can be developed to obtain areal spectral surface albedo data from albedo measurements at a certain flight altitude.

[28] The origin of the nonlinearity is due to the vertically inhomogeneous distribution of the particle microphysical properties. If the aerosol would be well-mixed throughout the whole troposphere (as the air which is responsible for Rayleigh scattering) then the smooth profile would lead to a much more linear variation of the albedo with altitude. As a proof, further calculations have been done (not shown)

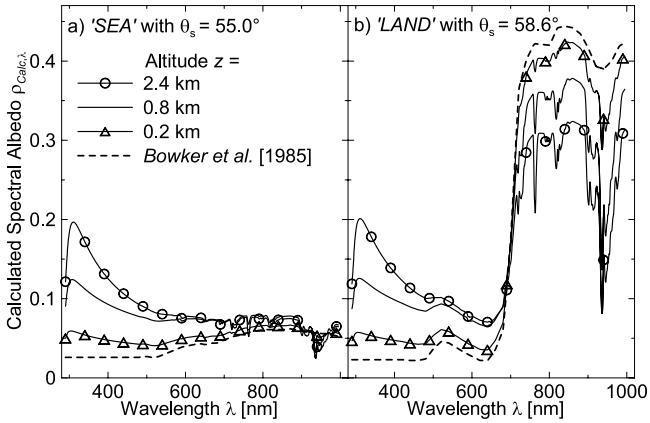

Figure 3. CALCULATED spectral albedo $\rho_{Calc,\lambda}$ (ratio of upward and downward calculated irradiances $F_{Calc,\lambda}\uparrow$ and $F_{Calc,\lambda}\downarrow$) as a function of wavelength λ for the three exemplarily altitudes $z = 2.4$ km, $z = 0.8$ km, and $z = 0.2$ km. Additionally the surface albedo data by *Bowker et al.* [1985] are plotted as dashed lines (type 'water' in Figure 3a and type 'grass' in Figure 3b). Aerosol particles and gas molecules are included in the calculations. θ_s represents the solar zenith angle. Figure 3a depicts the case '*SEA*', Figure 3b shows calculations for the case '*LAND*'.

assuming a vertically constant particle profile throughout the whole troposphere. For the vertically constant aerosol, the albedo changes more rapidly with height than in the Rayleigh atmosphere, but the change is almost linear. On the contrary, if the aerosol profile is not constant, as is the case in the real atmosphere, the albedo profile becomes more and more nonlinear. This explanation underlines even more that the aerosol profile below the aircraft needs to be known in order to accurately determine surface albedo from aircraft measurements.

[29] In Figure 3, spectra of the calculated albedo are presented for the two measurement cases '*SEA*' and '*LAND*', and for the three selected altitudes $z = 2.4$ km (open circles), $z = 0.8$ km (solid lines), and $z = 0.2$ km (open triangles). The three altitudes represent the conditions in the free troposphere, below the temperature inversion, and near the surface, respectively (see Figure 1). The curves depict the results including scattering and absorption of atmospheric gases and aerosol particles in the radiative transfer calculations. Additionally the spectral surface albedo functions assumed in the calculations are shown as dashed lines. For the case '*SEA*' (Figure 3a) the spectral albedo continuously increases with altitude. For the case '*LAND*' (Figure 3b) there is a different behavior. For wavelengths larger than about 700 nm the spectral albedo decreases with increasing altitude, which is opposite to the vertical pattern below this wavelength.

[30] In both cases there is a local maximum (spectral peak) in the curves around 310 nm wavelength in Figure 3, which becomes less obvious and which shifts to lower wavelengths with decreasing altitude. The reason for this spectral peak is the combined effect of Rayleigh scattering, which decreases as the wavelength increases, and of ozone absorption, which has its maximum at ~255 nm and decreases for longer wavelengths. Above 320–330 nm wavelength, ozone absorption may be neglected and therefore the reflectivity of the atmosphere increases towards smaller wavelengths, and so does the spectral albedo. Starting around 320 nm towards lower wavelengths ozone absorption becomes significant enough to reduce the reflectivity; below about 310 nm wavelength the atmospheric reflectivity drops quickly because of the near-exponential increase of ozone absorption. In order to look at the details, the ratio of the global downward irradiance at high altitude to that at a lower altitude was analyzed (not shown). The same altitude ratio was calculated for the diffuse upward irradiances. The altitude ratio of the global downward irradiances steadily increase with decreasing wavelength which is clearly due to ozone absorption. However there is no spectral peak in the altitude ratio for the global downward irradiances. On the other hand, the altitude ratio for the diffuse upward spectral irradiances clearly shows the relative maximum at short wavelengths which causes the spectral peak in the albedo at high altitudes. Hence, this peak is indeed caused by the wavelength dependence of Rayleigh scattering versus ozone absorption. But it is the diffuse upward reflection of the lower layer which affects the diffuse upward irradiance causing the spectral albedo peak, rather than the downward irradiance. This interpretation is supported by additional calculations with ozone absorption switched off (A. Kylling, private communication).

[31] The results in Figures 2 and 3 underline the urgent need to correct the albedo measurements at a certain flight altitude to retrieve the areal spectral surface albedo. Even measurements of the spectral albedo at 0.2 km above the surface would be biased by atmospheric scattering and absorption between the surface and the flight level. The ratio between the spectral albedo at 0.2 km altitude and that at the ground drops from a maximum value of 2.3 at 305 nm wavelength to about 1.07 at 880 nm for the case '*SEA*' (not shown). Over '*LAND*' this ratio is slightly different (2.5 at 305 nm; 0.96 at 880 nm wavelength).

[32] Figure 4 compares the simulation results considering scattering and absorption due to aerosol particles and gas molecules (solid lines with open symbols) with those

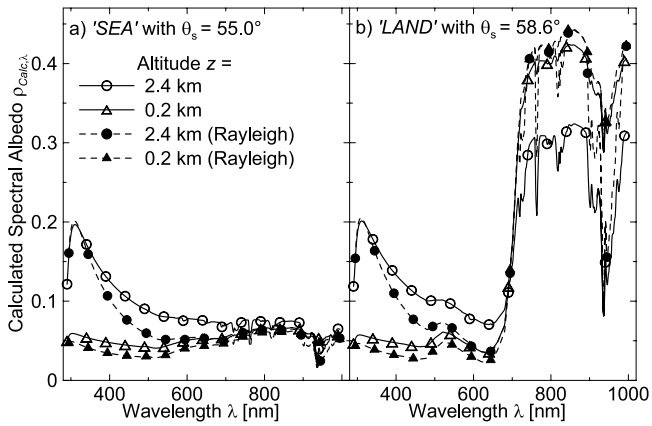

Figure 4. The same as Figure 3 but for the two altitudes $z = 2.4$ km and $z = 0.2$ km, only. In addition calculation results are added for a pure Rayleigh atmosphere as dashed lines with solid symbols. θ_s represents the solar zenith angle. Figure 4a depicts results of the calculations for the case '*SEA*', Figure 4b shows results calculated for the case '*LAND*'.

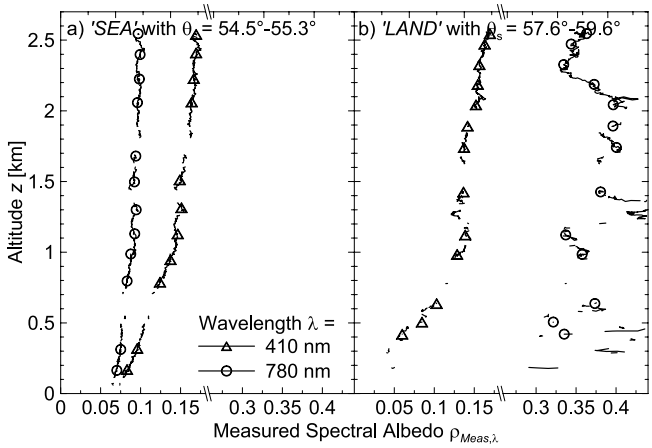

Figure 5. The same as Figure 2 but the MEASURED profiles of spectral albedo $\rho_{Meas,\lambda}$ (ratio of measured upward and downward irradiances $F_{Meas,\lambda}\uparrow$ and $F_{Meas,\lambda}\downarrow$) as a function of altitude z are shown. θ_s represents the solar zenith angle. The data result from the measurement cases '*SEA*' (Figure 5a) and '*LAND*' (Figure 5b), respectively. The measurements stem from the NORTH-SEA-2000 campaign (September 23, 2000).

obtained assuming a Rayleigh atmosphere (dashed lines with solid symbols) for two altitudes. Outside of the strong gas absorption bands (mainly O_2 and H_2O) the differences between the spectral albedo of an aerosol-loaded and that of a pure Rayleigh atmosphere are significant over most parts of the considered wavelength range. For increasing wavelengths the albedo of a Rayleigh atmosphere approaches the values of the surface albedo because the Rayleigh optical depth becomes smaller. Within the O_2 and H_2O gas absorption bands the differences between the surface albedo and that of the Rayleigh atmosphere increase with altitude, representing the influence of oxygen and water vapor in the atmospheric layer below the considered altitude.

3.2. Experimental Data

[33] In this subsection measured profiles of spectral albedo $\rho_{Meas,\lambda}$ for the two cases '*SEA*' and '*LAND*' are presented. Profiles of measured albedo for two fixed wavelengths are depicted in Figure 5; spectra of measured albedo averaged over three height intervals are presented in Figure 6.

[34] The profile data are shown for the two wavelengths 410 nm (open triangles) and 780 nm (open circles) in Figure 5. The gaps in the solid lines result from the limitations of the horizontal stabilization of the Albedometer. Data are not accepted if the horizontal stabilization is out of its angular adjustment range (±6°) or other limitations (e.g., with regard to allowed accelerations).

[35] For the measurement case '*SEA*' (Figure 5a) the profiles are smooth and qualitatively similar to the calculated data in Figure 2a. The measured spectral albedo for 780 nm wavelength is smaller compared to that of 410 nm, which is in general agreement with the calculations. The enhanced nonlinearity of the profiles below the temperature inversion, which is most obvious in the calculations for the wavelength of 410 nm (Figure 2a) is also evident in the measurements. The measured profiles at wavelengths less than 410 nm show an even more nonlinear behavior below the temperature inversion (not shown).

[36] For the measurement case '*LAND*' (Figure 5b) there are strong fluctuations in the spectral albedo profiles due to inhomogeneities in the reflectance of the underlying surface over land. This is especially true for the profile measurement at the fixed wavelength of 780 nm, a wavelength where the albedo is highly dependent on the vegetation state. The gaps in the profiles due to the limitations of the horizontal stabilization are more frequent, mostly due to higher atmospheric turbulence (and related higher accelerations) observed in the measurement case '*LAND*'. This causes the horizontal stabilization to exceed its technical limitations more frequently than in the case '*SEA*' with less turbulence. Nevertheless, these data also agree qualitatively with the respective calculations (Figure 2b). The nonlinearity below the temperature inversion for 410 nm is obvious and the larger values of the surface albedo at 780 nm are also in agreement with the calculations.

[37] The measured albedo spectra (averaged over certain altitude intervals Δz) are shown in Figure 6. It reveals a similar pattern compared to the respective calculations (Figure 3), i.e., a continuous increase of the spectral albedo with increasing altitude for the case '*SEA*' and a reversal of this pattern for wavelengths beyond the vegetation step for the case '*LAND*'. Even the influence of the decrease of the oxygen and water vapor amount with decreasing altitude is evident in the gas absorption band regions of the measured spectral albedo. The reversal of the spectral trend of albedo with altitude for wavelengths of 400–500 nm, as reported by *Webb et al.* [2000], is also confirmed in Figure 6. The 'Near Surface' albedo data (open triangles with solid lines) show a more or less continuous increase with increasing

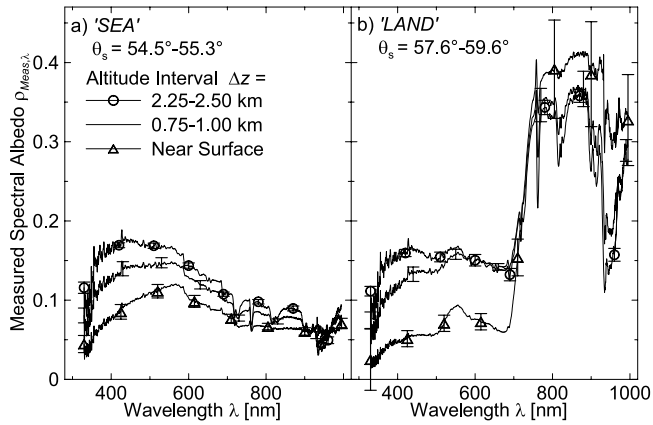

Figure 6. The same as Figure 3 but the MEASURED spectral albedo $\rho_{Meas,\lambda}$ (ratio of measured upward and downward irradiances $F_{Meas,\lambda}\uparrow$ and $F_{Meas,\lambda}\downarrow$) as a function of wavelength λ is shown. The spectra are averaged over different altitude ranges Δz. Vertical bars represent the standard deviation of the measurements. The 'Near Surface' data correspond to altitude averages over Δz = 50–300 m for the case '*SEA*' (Figure 6a) and Δz = 200–450 m for the case '*LAND*' (Figure 6b). θ_s represents the solar zenith angle. The measurements stem from the NORTH-SEA-2000 campaign (September 23, 2000).

wavelength (for λ between 400 nm and 500 nm), whereas this trend is reversed for the data obtained at higher flight levels.

[38] The standard deviations of the measurements are calculated via Gaussian error propagation from the standard deviations of the upward and downward spectral irradiances along the flight track. They are indicated as vertical bars in Figure 6. The standard deviations reveal a distinct decrease of the variability of the measured spectral albedo with increasing altitude. For the case '*SEA*' the standard deviations are generally small, for the case '*LAND*' they are higher especially beyond the vegetation step. The variability of the measured spectral albedo is mainly caused by the variability of the surface properties while the atmospheric properties might be considered constant throughout the aircraft descent. The higher up in the atmosphere, the larger is the smoothing influence of the atmosphere compared to that of the more variable surface, and therefore the smaller the influence of surface variability on the albedo measured at a certain height.

[39] The qualitative course of the measured spectral albedos in Figure 6 differs from the calculations (Figure 3) especially for wavelengths below 400 nm. Whereas the measured albedo spectra decrease below 400 nm with decreasing wavelength, the calculated ones increase. These qualitative differences mainly result from unrepresentative assumptions of the spectral surface albedo in the radiative transfer calculations. The assumed surface albedo functions provided by *Bowker et al.* [1985] do not fit in the actual circumstances of the specific cases discussed here. The essence of the surface extrapolation method presented in section 4 is to match these differences by adjusting the spectral surface albedo, assumed in the calculations, such that measured and calculated spectra of albedo agree.

[40] The conclusion from the results shown in this section is that the spectral surface albedo cannot directly be obtained from airborne spectral albedo measurements at a certain flight altitude. The atmospheric scattering and absorption beneath the flight altitude (atmospheric masking) considerably influence the albedo measurements and therefore need to be removed. A respective correction method requires vertical profiles of the aerosol microphysical or optical properties which cause deviations from a linear pattern in the profiles of the spectral albedo. As a consequence a nonlinear method is described in the following section, which extrapolates the spectral albedo measurements at a certain flight level to the surface to retrieve the areal spectral surface albedo.

4. Nonlinear Surface Extrapolation Method

4.1. Methodology

[41] The problem is to derive the spectral surface albedo $\rho_{Surf,\lambda}$ at the ground ($z = z_0 = 0$) from airborne measurements at a certain altitude z_{Flight}. For this purpose the influence of the atmospheric constituents (gas and particle absorption and scattering within the layer between z_0 and z_{Flight}) has to be described and the respective atmospheric masking must be removed. This is done by a nonlinear extrapolation of the aircraft measured global downward irradiances to the ground using radiative transfer calculations. These calculations have to be performed using the measured meteorological and aerosol particle properties within the layer between the surface and the flight level. Then, assuming a hypothetic guess for the surface albedo, the diffuse upward irradiances at the flight level are calculated. Afterward, the usual procedure would be to vary the spectral surface albedo until the calculated diffuse upward irradiances match with the measured diffuse upward irradiances. However, in this subsection analytic equations are derived which avoid such time consuming iterations. The final equation requires the calculated spectral albedos at the flight level and the surface, as well as the measured albedo at the flight level as input.

4.1.1. Equations

[42] In detail the method works as follows. In a first step the radiative transfer model calculates the spectral irradiances (global downward and diffuse upward, $F_{Calc,\lambda}\downarrow$ and $F_{Calc,\lambda}\uparrow$) as a function of altitude above ground z on the basis of the measured meteorological and aerosol microphysical input. It needs to be checked that the measured and calculated spectra of the global downward irradiances at the flight level agree within the range of the measurement uncertainty, otherwise the case is excluded from further analysis. That means it needs to hold:

$$F_{Calc,\lambda}\downarrow\left(z_{Flight}\right) \cong F_{Meas,\lambda}\downarrow\left(z_{Flight}\right) \tag{1}$$

[43] This assumption can be fulfilled even without using the correct spectral surface albedo in the radiative transfer calculations due to the low sensitivity of the global downward irradiance with regard to surface albedo. A ±20% variation in spectral surface albedo (for a solar zenith angle of 56°) causes a change of less than ±0.6% in the global downward spectral irradiances at the surface, where this influence is expected to be maximum [see *Wendisch et al.*, 2002, Table 4]. This is less than the measurement uncertainty.

[44] In a second step the calculated spectral transmittance $\tau_{Calc,\lambda}$ of the layer between z_{Flight} and z_0 is derived from the simulated global downward irradiances by:

$$\tau_{Calc,\lambda} = \frac{F_{Calc,\lambda}\downarrow(z_0)}{F_{Calc,\lambda}\downarrow\left(z_{Flight}\right)} \tag{2}$$

Below it is assumed that the transmittance is independent of the spectral surface albedo, which is not a serious limitation under the cloudless conditions considered here. Because the global downward irradiances are only slightly affected by the assumed surface albedo, the transmittance is also not very sensitive to the choice of the surface albedo. With the help of $\tau_{Calc,\lambda}$ the measured global downward irradiance at the flight level $F_{Meas,\lambda}\downarrow$ (z_{Flight}) is extrapolated to the surface to yield the extrapolated global spectral downward irradiance at the surface $F_{Ext,\lambda}\downarrow$ (z_0) by:

$$F_{Ext,\lambda}\downarrow(z_0) = F_{Meas,\lambda}\downarrow\left(z_{Flight}\right)\cdot\tau_{Calc,\lambda} \tag{3}$$

This is the first quantity needed to retrieve the areal spectral surface albedo from the measurements at the flight level. The second quantity, the extrapolated diffuse spectral upward irradiance at the surface $F_{Ext,\lambda}\uparrow$ (z_0), is calculated in the third step of the method assuming that the ratio

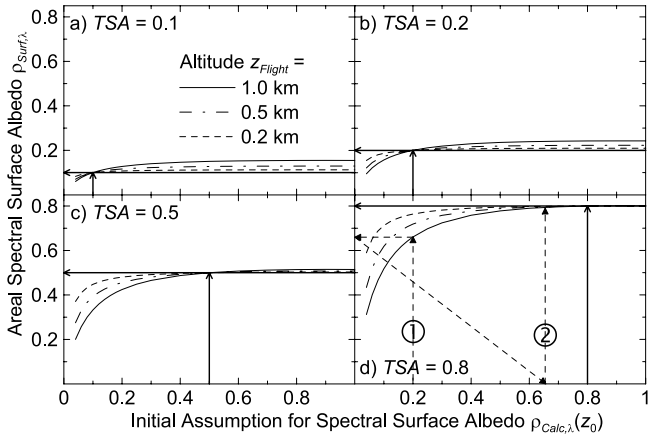

Figure 7. Retrieved areal spectral surface albedo $\rho_{Surf,\lambda}$ as a function of the initial assumption for the spectral surface albedo $\rho_{Calc,\lambda}$ (z_0) (see equation (6)). The three graphs in each panel depict the results for different flight levels. Figures 7a to 7d represent the calculations for varying values of the "True" Surface Albedo (TSA), indicated by solid arrows. The wavelength for the calculations is 410 nm, the solar zenith angle is fixed at 32°. The columnar particle optical thickness is set to 0.5, the total optical thickness (particles plus Rayleigh) below 1 km altitude is 0.27. The dashed arrows in Figure 7d are included to demonstrate how the technique works in an iterative manner.

between diffuse upward irradiances at the surface and at the flight level is identical for both the measurements (or extrapolated measurements) and the calculations, i.e.:

$$\frac{F_{Ext,\lambda}\uparrow(z_0)}{F_{Meas,\lambda}\uparrow(z_{Flight})} = \frac{F_{Calc,\lambda}\uparrow(z_0)}{F_{Calc,\lambda}\uparrow(z_{Flight})} \tag{4}$$

It should be noticed that the measured and calculated diffuse upward irradiances are not assumed to agree within the measurement uncertainty (as it is requested for the global downward irradiances). Instead the differences between $F_{Meas,\lambda}\uparrow$ (z_{Flight}) and $F_{Calc,\lambda}\uparrow$ (z_{Flight}) are related to the differences between the real surface albedo and that assumed in the calculations. In this way the surface albedo is adjusted such that the calculated diffuse upward irradiances at the flight level match the respective calculations of $F_{Calc,\lambda}\uparrow$ (z_{Flight}). This matching works because the global downward irradiances at the flight level and the layer transmittance only minimally depend on the surface albedo assumed in the calculations.

[45] In the fourth step of the method the desired areal spectral surface albedo $\rho_{Surf,\lambda}$ is obtained from the ratio between extrapolated upward and downward spectral irradiances at the surface. The measured and calculated spectral irradiances (diffuse upward and global downward) and the calculated transmittance are combined to yield:

$$\rho_{Surf,\lambda} = \frac{F_{Ext,\lambda}\uparrow(z_0)}{F_{Ext,\lambda}\downarrow(z_0)} = \frac{F_{Calc,\lambda}\uparrow(z_0)}{F_{Calc,\lambda}\uparrow(z_{Flight})} \cdot F_{Meas,\lambda}\uparrow(z_{Flight}) \cdot \frac{1}{F_{Meas,\lambda}\downarrow(z_{Flight})\cdot\tau_{Calc,\lambda}} \tag{5}$$

Notice that if measured and calculated quantities are equal in equation (5) then the definition equation for the measured surface albedo remains. Combining the above equations yields the final expression for the areal spectral surface albedo:

$$\rho_{Surf,\lambda} = \frac{\rho_{Calc,\lambda}(z_0)}{\rho_{Calc,\lambda}(z_{Flight})} \cdot \rho_{Meas,\lambda}(z_{Flight}) \tag{6}$$

[46] In the following text this procedure is called the nonlinear surface extrapolation method. For a fixed flight altitude z_{Flight}, equation (6) implies a linear relationship between surface albedo $\rho_{Surf,\lambda}$ and measured albedo at the flight level $\rho_{Meas,\lambda}$ (z_{Flight}). However, since z_{Flight} is not necessarily a constant, equation (6) holds for any flight altitude z_{Flight}. Therefore the terms in equation (6) are nonlinear, mainly because of the transmittance term $\tau_{Calc,\lambda}$ (an exponential function). The nonlinearity of $\rho_{Calc,\lambda}$ is clearly illustrated in Figure 2, and that of $\rho_{Meas,\lambda}$ in Figure 5.

[47] This nonlinear surface extrapolation method is a simple and efficient approach which avoids complicated inverse algorithms usually applied to retrieve surface albedo from satellite data [e.g., *Jin et al.*, 2003]. These inverse techniques correct for atmospheric masking of the received satellite signal by minimizing the squared errors between the satellite observed reflectance and that predicted by iterative radiative transfer simulations. In the nonlinear surface extrapolation method presented here typically only one run of the radiative transfer model is required. It should be noted that bidirectional surface properties cannot be derived from the method presented in this paper.

4.1.2. Sensitivity to Initial Surface Albedo Assumption

[48] The described method requires an initial assumption of the spectral surface albedo for the radiative transfer calculations. A sensitivity study has been performed in order to check how the choice of this guess for the surface albedo influences the spectral surface albedo retrieved from the nonlinear surface extrapolation method. For this study the libRadtran radiative transfer model by A. Kylling and B. Mayer (manuscript in preparation, 2004) was used. libRadtran is a flexible and user-friendly model package which allows quick, yet accurate simulation of the quantities needed for the sensitivity purposes. For this application, the discrete ordinate solver DISORT by *Stamnes et al.* [1988] was used. The simulations were conducted for the two solar zenith angles 32° and 55° and for two wavelengths, 410 nm and 780 nm. The midlatitude summer profile by *Anderson et al.* [1986] and the spring-summer rural aerosol profile by *Shettle* [1989] were used for the calculations. A range of aerosol optical thicknesses from 0 to 1 was covered. In a first step synthetic measurements of upward and downward spectral irradiances at the flight altitude were simulated using the "True" Surface Albedo (TSA) in the radiative transfer calculations. In the second step the nonlinear surface extrapolation method was applied to these synthetic data, using start values (initial guess) of the surface albedo between 0.03 and 1.0. A respective example plot of the results is shown in Figure 7 (for a solar zenith angle of 32° and a wavelength of 410 nm). The simulations in this figure were done for a columnar (vertically integrated over the whole atmosphere) particle optical thickness of 0.5. The particle optical thickness below 1 km altitude is 0.235 for this case, which results in a value of about 0.27

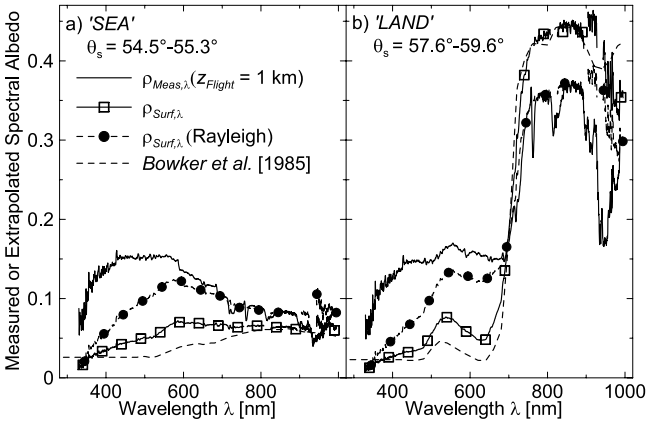

Figure 8. Measured and extrapolated albedo as a function of wavelength λ. The solid curves without symbols correspond to the spectral albedo measurements taken at 1 km altitude [$\rho_{Meas,\lambda}$ (z_{Flight} = 1 km)]. The solid curves with open squares [$\rho_{Surf,\lambda}$] show the results applying the nonlinear surface extrapolation method (equation (6)). The extrapolation results obtained for a Rayleigh atmosphere are included as dashed lines with solid circles [$\rho_{Surf,\lambda}$ (Rayleigh)]. For comparison the spectral surface albedo data by *Bowker et al.* [1985] are included (type 'water' in Figure 8a and type 'grass' in Figure 8b). θ_s represents the solar zenith angle. Figure 8a depicts data collected for the case '*SEA*', Figure 8b shows results obtained for the case '*LAND*'. The measurements stem from the NORTH-SEA-2000 campaign (September 23, 2000).

for the total optical thickness (particles plus Rayleigh) below 1 km.

[49] The curves in Figure 7 are the results for three different flight altitudes (0.2 km, 0.5 km, and 1.0 km), the four panels represent the different TSA values (0.1; 0.2; 0.5; 0.8). If the assumed surface albedo is identical to the TSA value, then the retrieved areal spectral surface albedo perfectly matches the true surface albedo TSA. Therefore all curves cross each other in all four panels. In practice, the initially assumed albedo is not known and therefore will differ from TSA. However, the figure clearly shows that, if the surface albedo guess is not too different from TSA, only small deviations between the retrieved surface albedo and TSA occur (see difference between the horizontal solid arrows and the respective curves).

[50] As expected, the error in the retrieved surface albedo decreases with decreasing flight altitude. The lower the airborne observations are performed, the less is the masking effect of the atmosphere between flight level and ground, and the less problems arise in the retrieval. The retrieval error is largest above highly reflecting ground (large TSA values) if very low initial values of $\rho_{Calc,\lambda}$ (z_0) are assumed. Considering these results, it seems reasonable to use an intermediate start value like 0.5 for the initial albedo guess if nothing is known about the reflection properties of the underlying surface. However, for most applications at least the general type of reflecting surface (sea, land, or snow) is known. Based on this knowledge reasonable literature data [e.g., *Bowker et al.*, 1985] can be used for the initial surface albedo guess. These data should be close enough to the "True" spectral surface albedo and therefore errors in the retrieved surface albedo due to the initially guessed surface albedo are sufficiently small.

[51] The shape of the curves also suggests that the method will quickly converge against the correct surface albedo value TSA, if the method is used in an iterative manner (repeating the retrieval with the derived surface albedo as initial value). This is illustrated by the dashed arrows in Figure 7d (TSA = 0.8). If an initial guess of 0.2 is assumed for the spectral surface albedo (step 1 of iteration), then a value of 0.66 (instead of 0.8) is retrieved by the nonlinear surface extrapolation method. If this result is used in step 2 of the iteration, a surface albedo of about 0.79 is retrieved, which is sufficiently close to the correct one.

[52] If a solar zenith angle of 55° is used instead of 32° the results of the sensitivity calculations are nearly identical to those shown in Figure 7. For 780 nm wavelength the sensitivity of the retrieved areal spectral surface albedo with regard to the initial guess is smaller compared to the results for 410 nm. Therefore it is concluded that the method is sufficiently robust against the initial guess of the albedo. Using the technique iteratively is possible but not needed if the measurements are done at low flight altitudes and the general character of the reflecting surface is known.

[53] Further sensitivity tests indicate, that the assumptions for the optical properties of the atmosphere above the flight layer have only little influence on the retrieval results. Even if a homogeneous cloud layer is placed above z_{Flight}, the derived surface albedo does not change significantly, compared to the cloudless retrieval result. The major impact stems from the optical properties of the atmosphere below flight level. Therefore, unless further sensitivity tests have been performed, the approach cannot be applied for satellite retrievals, where usually the crucial information on optical properties of the atmosphere below the satellite is missing.

[54] Please note that the derived uncertainties, shown in Figure 7 address only the performance of the retrieval itself, but do not include measurement uncertainties, neither in the spectral irradiance nor the atmospheric properties.

4.1.3. Gas Absorption Bands

[55] The extreme strong gradient of the spectral albedo within the major gas absorption bands combined with unavoidable absolute and wavelength setting measurement uncertainties produce some artificial spikes in the extrapolated areal spectral surface albedos in the gas absorption bands. Therefore, in the subsequent graphs the results of the nonlinear surface extrapolation method within the following spectral ranges have been omitted: 756–764 nm (O_2 absorption band), 808–825 nm, 894–904 nm, 928–943 nm (H_2O absorption bands) for both the Albedometer and SSFR data. For the SSFR measurements additionally the spectral absorption bands of H_2O for 1100–1170 nm and 1300–1510 nm have been excluded from the retrieval.

4.2. Illustration of the Method

[56] To further explain the nonlinear surface extrapolation method, the technique is applied to the two specific cases '*SEA*' and '*LAND*' introduced in subsection 2.3. The results are illustrated in Figure 8. The measured spectral albedos for the two cases '*SEA*' and '*LAND*' at an altitude of

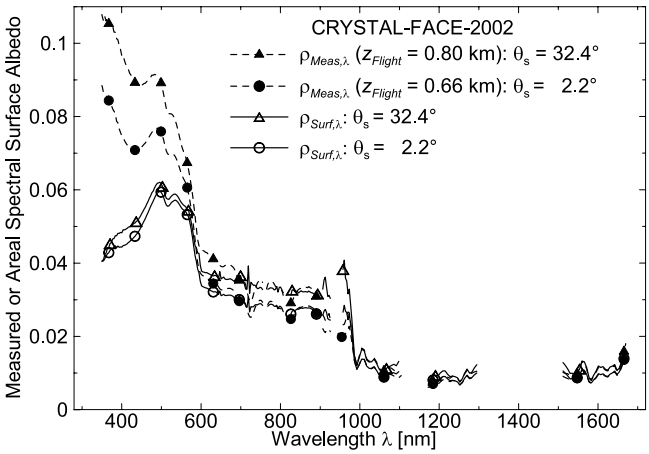

Figure 9. Measured spectral albedo $\rho_{Meas,\lambda}$ for the two flight altitudes with different solar zenith angles θ_s. Furthermore areal spectral surface albedo $\rho_{Surf,\lambda}$ are shown obtained by applying the nonlinear surface extrapolation method (equation (6)). The data were taken over SEA surfaces during CRYSTAL-FACE-2002 (July 16 and 21, 2002).

z_{Flight} = 1 km are plotted as solid lines. Using the output of the radiative transfer model, the extrapolated areal spectral surface albedos are plotted as solid lines with open squares. Clearly there are differences between the spectral surface albedos from literature [*Bowker et al.*, 1985], which are additionally shown as dashed lines in Figure 8. For the case '*SEA*' the literature data of surface albedo are mostly lower compared to the results of the nonlinear surface extrapolation method throughout most of the spectral range considered here. For the case '*LAND*' this also holds for wavelengths less than the vegetation step (about 700 nm). The maximum in the green color of the albedo spectra is obvious in both the literature data and the results of the nonlinear surface extrapolation method. The vegetation step itself is more steep in the literature data compared to the results of the nonlinear surface extrapolation method. Beyond 700 nm wavelength the literature data agree well with the nonlinear surface extrapolation method results up to 870 nm, above that wavelength some differences are obvious, which are partly a result of increasing measurement uncertainties towards the spectral end of the sensitivity of the detection unit.

[57] Additionally the dashed lines with solid circles in Figure 8 show the results of the nonlinear surface extrapolation method assuming a Rayleigh atmosphere in the radiative transfer calculations. The resulting extrapolated areal surface albedo shows significant differences from both the literature data and the results of the nonlinear surface extrapolation method including aerosol particles, which again stresses the need to include the aerosol particle microphysical properties in the nonlinear surface extrapolation method.

5. Examples of Averaged Areal Spectral Surface Albedo

[58] In this section areal spectral surface albedo data obtained over different sea and land surfaces in three measurement campaigns are presented. To all of these data the nonlinear surface extrapolation method is applied. The data are used to discuss the dependence of spectral surface albedo on solar zenith angle, the small-scale and general variability of the spectral surface albedo. Finally, typical data of the spectral surface albedo for different sea and land surfaces are given in parameterized form.

[59] A large amount of spectral irradiance measurements were collected during the three experiments. The upward and downward irradiance spectra were averaged over time intervals less than 10 min, which corresponds to a maximum change in solar zenith angle of 2°. From the averaged irradiances the albedo was calculated. Only those albedo data are selected for detailed analysis where the standard deviation of the spectral downward irradiances (within the maximum 10-min averaging period) is less than 2%. This empirical threshold value is used to exclude contamination of the data set by cirrus clouds above the flight altitude, which significantly increase the variability of the measured downward irradiances. It is based on experimental experience gathered during the flights. Furthermore, only those cases are analyzed for which the calculated spectra of global downward irradiances agreed with the measurements within their error bars.

5.1. Dependence on Solar Zenith Angle

[60] Usually lowest values of surface albedo are observed around noon and sometimes an asymmetric behavior of the daily cycle of surface albedo is observed [*Grant et al.*, 2000]. Appropriate data on this subject are limited in our study, therefore the dependence of the retrieved areal spectral surface albedo on solar zenith angle is only briefly discussed for measurements taken during the CRYSTAL-FACE-2002 campaign. Because of the high variability of the spectral surface albedo over land, only measurements collected over sea are shown in this regard.

[61] Figure 9 depicts airborne measurements of the spectral albedo (dashed lines), obtained for two different days over sea, together with the retrieved spectral surface albedos (solid lines). The measurements were taken at different solar zenith angles and altitudes. The mixed effect of both factors becomes obvious in the albedo measurements especially for wavelengths less than 600 nm. For the larger solar zenith angle and higher altitude (solid triangle) the measured spectral albedo is larger compared to the case with nearly overhead Sun (solid circles). This is in agreement with the expectations from radiative transfer calculations. However, the retrieved spectral surface albedo of the two cases is similar. Only a small solar zenith angle dependence is observed with slightly higher values for the larger solar zenith angles. This coincides with findings by *Webb et al.* [2000], and *Aoki et al.* [2002]. For wavelengths larger than 600 nm the solar zenith angle dependence is larger compared to lower wavelengths, which can be interpreted as an effect of the relative increase of elastic scattering within the ocean [*Gordon*, 1999]. However, both conclusions are based on two cases only, with two values of solar zenith angle θ_s, covering the range from 2.2°–32.4° which corresponds to $\mu = \cos\theta_s = 0.999–0.844$. For smaller μ-values changes may be much more significant.

[62] A remarkable feature of the retrieved spectral surface albedo in Figure 9 is the obvious maximum around 500 nm

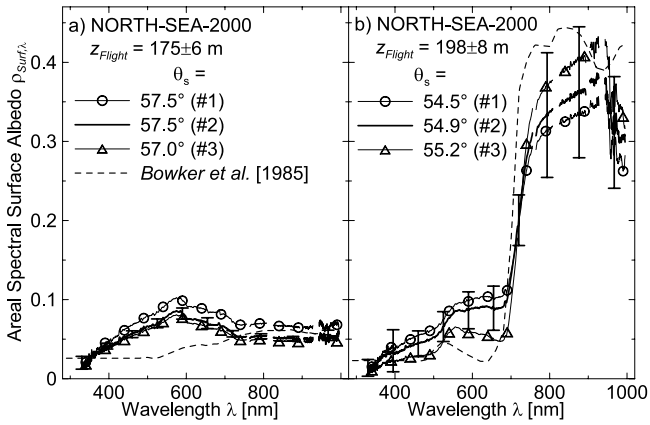

Figure 10. Areal spectral surface albedo $\rho_{Surf,\lambda}$ averaged along triangular horizontal flight legs (labeled #1, #2, #3) flown over sea (Figure 10a) and land (Figure 10b). The vertical bars represent the standard deviation of the measurements along flight leg #2 as an example. Spectral surface albedo data by *Bowker et al.* [1985] are shown in addition as dashed lines (type 'water' in Figure 10a and type 'grass' in Figure 10b). θ_s represents the solar zenith angle. The measurements stem from the NORTH-SEA-2000 campaign (Figure 10a: Over sea, September 24, 2000; Figure 10b: Over land, September 22, 2000).

wavelength. The shape of this maximum is in good agreement with figures reported by *Ohlmann et al.* [2000]. These authors interpret this spectral feature as the influence of chlorophyll-a within the ocean and try to use this signature to retrieve the chlorophyll-a concentration near the ocean surface.

5.2. Small-Scale Variability

[63] In this subsection low-level measurements (z_{Flight} < 200 m) of spectral surface albedo over sea and land are presented to look at its small-scale variability. The restriction to low flight altitudes minimizes the possible influence of spatial atmospheric inhomogeneities, although their influence is assumed to be low. In this way the small-scale variability of the areal spectral surface albedo is clearly related to the surface and the atmospheric variability can be neglected. The measurements discussed in this subsection stem from the NORTH-SEA-2000 campaign.

[64] Two near-surface flights were conducted over sea on September 24, 2000 (z_{Flight} = 175 ± 6 m) and over land on September 22, 2000 (z_{Flight} = 198 ± 8 m). A horizontal, triangular flight pattern was chosen for both flights with leg lengths of about 10 km (150 s). The airborne albedo measurements are averaged over the flight legs and the extrapolated areal spectral surface albedos are indicated as #1, #2, and #3 in Figure 10. The data obtained over sea are presented in Figure 10a, those retrieved over land are shown in Figure 10b. For the flight leg #2 of the triangular flight patterns (thick solid lines) the spectral standard deviation of $\rho_{Surf,\lambda}$ are indicated as vertical bars.

[65] Over sea (Figure 10a) two of the measurements (#2 and #3, solid line and open triangles) are close to each other and within the variability bars of the leg #2 measurements. The data retrieved for the measurements along leg #1 are outside the vertical bars. One possible explanation is an increase of near surface wind speed during the measurements on flight leg #1 as compared to the flight legs #2 and #3 which would systematically increase the swell (more white caps) and hence the albedo. This suspicion is supported by the higher variability (i.e., higher standard deviations) of the retrieved areal sea surface albedo along flight leg #1 (not shown). Further reason for the differences could be a different sea depth or another ocean water composition. Solid evidence for these interpretations cannot be given. It should be noticed that, especially for wavelengths less than 700 nm, the retrieved areal surface albedo for all three flight legs is significantly larger than the respective literature values by *Bowker et al.* [1985] (dashed line).

[66] Over land (Figure 10b) the averaged areal surface albedo differs for the three flight legs and is also highly variable as can be seen from the vertical bars (standard deviations) shown for leg #2 data (solid line). The data for leg #3 (open triangles) depict a distinct peak of green reflectivity, while leg #1 (open circles) was obviously mostly over surface with less living vegetation. For all the three legs the vegetation step around 700 nm is less steep compared to the respective literature data from *Bowker et al.* [1985].

[67] Altogether it becomes obvious from Figure 10 that the small-scale variability of the areal spectral surface albedo can be substantial especially over land surfaces. Even over sea, differences can be observed.

5.3. Typical Areal Spectral Surface Albedos

[68] Not each radiation measurement campaign can afford a detailed characterization of the areal spectral surface albedo, because either the instrumentation or the appropriate data are not available. Also the spectral details of the surface albedo may not always be that important for the specific purpose of the campaign. Therefore, averaged areal spectral surface albedo data are presented in this section, as derived from the three airborne measurements campaigns. Parametrization formula of the averaged areal spectral surface

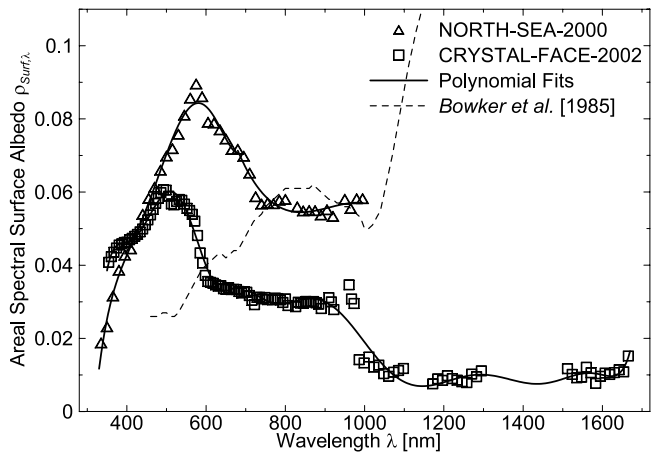

Figure 11. Typical areal spectral surface albedo over different sea surfaces. For the NORTH-SEA-2000 data only each 30th spectral data point is shown, for the CRYSTAL-FACE-2002 data only each 2nd spectral data point is plotted. The solid lines represent the respective parametrization using equation (7). Additionally spectral surface albedo data by *Bowker et al.* [1985] (type 'water') are plotted as dashed line.

Table 2. Polynomial Coefficients for the Parametrization of the Areal Spectral Surface Albedo After Equation (7) for Typical Data Collected Over Different Sea Surfaces[a]

	NORTH-SEA-2000: $\theta_s = 54°-56°$		CRYSTAL-FACE-2002: $\theta_s = 2°-32°$	
$\lambda =$	330–680 nm	680–995 nm	350–680 nm	680–1670 nm
a_0	−7.585936765	1.367923293	−55.02673544	−764.5088631
a_1	0.07839225068	−0.004374769196	0.6756944893	6.499386024
a_2	−0.0003205014374	4.831247709E-006	−0.003410924551	−0.02421321231
a_3	6.48266704E-007	−1.767407524E-009	9.061568585E-006	5.188542608E-005
a_4	−6.454213098E-010	0	−1.335596483E-008	−7.048714285E-008
a_5	2.525136682E-013	0	1.035474321E-011	6.29732813E-011
a_6	0	0	−3.300065817E-015	−3.701254093E-014
a_7	0	0	0	1.380680151E-017
a_8	0	0	0	−2.96765682E-021
a_9	0	0	0	2.801858178E-025

[a]Double precision needed to reproduce the parametrization; θ_s represents the solar zenith angle.

albedos are supplied and in this way the measurements can be used to analyze data obtained in other experiments. The data are not postulated to be fully representative.

[69] For this purpose all available averaged retrieved areal spectral surface albedos are categorized into two specific surface types (sea and land), separately for each of the three campaigns (NORTH-SEA-2000, BBC-2001, CRYSTAL-FACE-2002). Then these data are averaged again and parameterized using n'th order polynomials:

$$\rho_{Par,\lambda} = \sum_{i=0}^{n} a_i \cdot \lambda^i \tag{7}$$

where a_i are the polynomial coefficients. λ represents the wavelength given in units of nm. The parametrization was performed manually balancing the two needs of capturing details of the measurements and keeping n as low as possible. Data within the strong absorption bands of O_2 and H_2O are not included in the spectral surface albedo retrieval (see discussion in section 4.1.3). However, in the parametrizations the spectral gaps in the retrieved data are covered. This approach is based on the reasonable assumption of spectral smoothness of retrieved areal surface albedo in the gas absorption bands.

5.3.1. Sea Surfaces

[70] In Figure 11 the typical spectral sea albedos obtained in the NORTH-SEA-2000 (open triangles) and the CRYSTAL-FACE-2002 (open squares) campaigns are presented. Additionally the reflectance for 'water' by *Bowker et al.* [1985] is plotted as dashed line. The areal spectral sea surface albedo from the CRYSTAL-FACE-2002 experiment is lower compared to the results of both the NORTH-SEA-2000 campaign and the 'water' albedo by *Bowker et al.* [1985] over most parts of the spectrum. The chlorophyll-a peak is obvious in both the NORTH-SEA-2000 and the CRYSTAL-FACE-2002 areal surface albedos, although the level is higher and the peak wavelength is shifted to larger wavelengths for the NORTH-SEA-2000 data set. The different level can only partly be explained by the generally much larger solar zenith angles during the NORTH-SEA-2000 measurements. Different swell, sea water constituents, and ocean ground albedo in shallow waters are further factors which can be responsible for the observed differences. The concentrations of water constituents depend strongly on time and location. In September the North Sea may contain significant amounts of particulate material, yellow substance and chlorophyll, whereas the coastal waters of Florida are probably less contaminated. Yellow substance and particulate material can be characterized by a strong decrease in absorption with increasing wavelength while chlorophyll has an absorption maximum at around 430 nm. The scattering of particulate material depends only slightly on wavelength. A combined effect of these water constituents can explain the features of the albedo observed during NORTH-SEA-2000. Altogether these differences in the sea areal surface albedo illustrate how variable this quantity can be for different oceans. The respective polynomial coefficients for the parameterized areal spectral surface albedo over sea are given in Table 2.

5.3.2. Land Surfaces

[71] Figure 12 presents the typical areal spectral surface albedos retrieved over land for the three measurement campaigns NORTH-SEA-2000 (open triangles), BBC-2001 (solid circles), and CRYSTAL-FACE-2002 (open squares). Whereas the results for the two first campaigns are similar especially beyond the so-called vegetation step around 700 nm wavelength, the CRYSTAL-FACE-2002 areal spectral surface albedo over land is lower. Again these

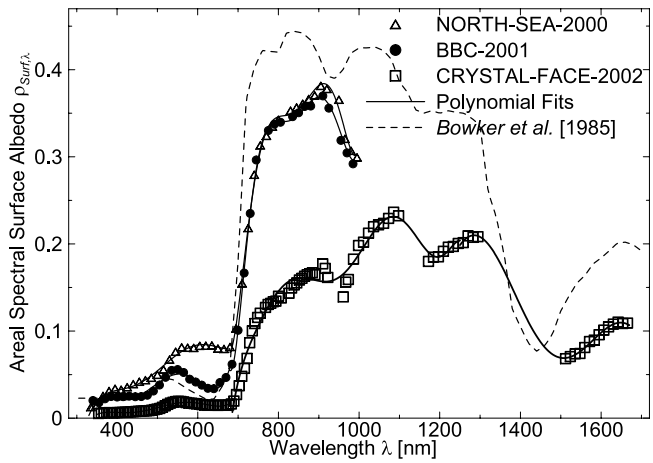

Figure 12. Typical areal spectral surface albedo over different land surfaces. For the NORTH-SEA-2000 and BBC-2001 data set only each 30th spectral data point is shown, for the CRYSTAL-FACE-2002 data only each 2nd spectral data point is plotted. The solid lines represent the respective parametrization using equation (7). Additionally spectral surface albedo data by *Bowker et al.* [1985] (type 'grass') are plotted as dashed line.

Table 3. The Same as Table 2, but for Data Collected Over Different Land Surfaces

	NORTH-SEA-2000: $\theta_s = 56°-60°$		BBC-2001: $\theta_s = 53°-56°$		CRYSTAL-FACE-2002: $\theta_s = 50°-52°$		
$\lambda =$	330–680 nm	680–995 nm	330–680 nm	680–995 nm	350–680 nm	680–1250 nm	1250–1670 nm
a_0	−12.01592121	10818.96608	−19.50426456	44397.33702	−6.951521737	−12704.59533	5072.432707
a_1	0.1229527427	−78.76334417	0.2099040549	−363.1534282	0.07280659467	111.0494365	−21.28314006
a_2	−0.0004950258216	0.2378698243	−0.0008893058741	1.266910169	−0.0003003839215	−0.4218648772	0.03695542723
a_3	9.803862042E-007	−0.0003815079998	1.854530472E-006	−0.002443703339	6.102129786E-007	0.0009095017488	−3.399157714E-005
a_4	−9.53157764E-010	3.427690569E-007	−1.902476674E-009	2.814734739E-006	−6.099606797E-010	−1.216858145E-006	1.746982622E-008
a_5	3.639843919E-013	−1.635905258E-010	7.682273056E-013	−1.936074553E-009	2.400725248E-013	1.034489449E-009	−4.757415466E-012
a_6	0	3.240433257E-014	0	7.363477684E-013	0	−5.456712798E-013	5.363917036E-016
a_7	0	0	0	−1.194583933E-016	0	1.632788192E-016	0
a_8	0	0	0	0	0	−2.12203679E-020	0
a_9	0	0	0	0	0	0	0

different levels cannot be explained with the generally smaller solar zenith angle during the CRYSTAL-FACE-2002 measurements, and thus represent significant variations of natural land surface reflection. The first two campaigns were both performed in September with much living vegetation at the surface. The CRYSTAL-FACE-2002 took place in July over a terrain which strongly dries out in summer. However, all three data sets show a much less pronounced vegetation step compared to the literature data by *Bowker et al.* [1985] (type 'grass'). The respective polynomial coefficients for the parameterized areal spectral surface albedos in Figure 12 are given in Table 3.

6. Summary and Conclusions

[72] Meteorological, aerosol microphysical and in particular spectral radiation data from three field campaigns are used to derive areal spectral surface albedos within the wavelength range from 330 to 1670 nm over different types of sea and land surfaces in cloudless atmospheric conditions. From calculations of profiles of the ratio between upward and downward spectral irradiances (spectral albedo) it is concluded that the vertical pattern of the albedo is not generally a linear function of height above ground. This nonlinearity is caused by the complex inhomogeneous profile of the aerosol properties. Therefore, a linear extrapolation of airborne spectral albedo measurements to the ground may lead to a bias in the retrieved areal surface albedo. As a consequence, a nonlinear surface extrapolation method is introduced. It includes spectral radiative transfer calculations, which require meteorological and aerosol microphysical input as well as measurements of the spectral albedo at a certain flight level. The need for a nonlinear surface extrapolation of the airborne albedo measurements to the ground to obtain the areal spectral surface albedo is motivated, and the influence of aerosol particle scattering and absorption between the flight level and the surface is proven to be significant.

[73] The areal surface albedo measurements, which are retrieved with the nonlinear surface extrapolation method from the data collected in the three field campaigns, are used to look at the solar zenith angle dependence of areal spectral surface albedo. From the limited data available (two measurement cases over sea, solar zenith angles between 2.2° and 32.4°) no clear conclusion on the dependence of the areal spectral surface albedo of solar zenith angle can be drawn in this paper. The small-scale variability as well as variations of areal surface albedo for different sea and land surfaces are investigated. The differences among the areal surface albedo measurements on the one hand, and the differences from the literature data reported by *Bowker et al.* [1985] on the other hand are significant. Literature data as those by *Bowker et al.* [1985], which are strictly applicable for distinct surface types only, may not always be appropriate to analyze radiation data from airborne field campaigns. Therefore, it is concluded that, for a detailed analysis of radiation data from specific radiation field experiments, a characterization of the specific spectral reflection properties of the underlying surface is unavoidable. However, if such data or the appropriate instrumentation is not available, typical areal spectral surface albedo data can be used, which are given for different sea and land surfaces in parameterized form in Tables 2 and 3.

[74] **Acknowledgments.** Part of this research was performed while one of the authors (M.W.) held a National Research Council Research Associateship Award at the NASA ARC. Dörthe Müller and Stephan Günnel (IfT) are acknowledged for their help in the Albedometer measurements. We are grateful to Warren Gore, Larry Pezzolo, and Tony Trias (NASA ARC) for their engineering and technical support during CRYSTAL-FACE-2002. As usual, the enviscope GmbH company and the pilot of the Partenavia, Bernd Schumacher, did an excellent job in preparing and conducting the measurements with the Partenavia. Arve Kylling (Norwegian Institute for Air Research, Norway), and Ann Webb (University of Manchester Institute of Science and Technology, UK) made useful comments on the manuscript. Jost Heintzenberg (IfT) has continuously supported this work. Funding by the German Science Foundation (DFG) and the German Research Ministry (BMBF) are acknowledged. Finally, we wish to thank the NASA Earth Science Enterprise Radiation Science Program for funding the CRYSTAL-FACE-2002 part of this research.

References

Anderson, G. P., S. A. Clough, F. X. Kneizys, J. H. Chetwynd, and E. P. Shettle (1986), AFGL atmospheric constituent profiles (0–120 km), *AFGL-TR-86-0110*, Air Force Geophys. Lab., Bedford, Mass.

Aoki, T., M. Masao, and L. Wenjian (2002), Spectral albedos of desert dust surfaces and size distributions of soil particles measured around Qira and Aksu in the Taklimakan Desert, *J. Arid Land Stud.*, *11*, 259–266.

Barker, H. W., et al. (2003), Assessing 1D atmospheric solar radiative transfer models: Interpretation and handling of unresolved clouds, *J. Clim.*, *16*, 2676–2699.

Blumthaler, M., and W. Ambach (1988), Solar UVB albedo of various surfaces, *Photochem. Photobiol.*, *48*, 85–88.

Bowker, D. E., R. E. Davis, D. L. Myrik, K. Stacy, and W. T. Jones (1985), Spectral reflectance of natural targets for use in remote sensing studies, *NASA Ref. Publ.*, *1139*.

Coulson, K. L., and D. W. Reynolds (1971), The spectral reflectance of natural surfaces, *J. Appl. Meteorol.*, *10*, 1285–1295.

Crewell, S., et al. (2004), The BALTEX Bridge Campaign: An integrated approach for a better understanding of clouds, *Bull. Am. Meteorol. Soc.*, in press.

Feister, U., and R. Grewe (1995), Spectral albedo measurements in the UV and visible region over different types of surfaces, *Photochem. Photobiol.*, *62*, 736–744.

Gordon, R. H. (1999), Contribution of Raman scattering to water leaving radiance: A reexamination, *Appl. Opt.*, *38*, 3166–3174.

Grant, I. F., A. J. Prata, and R. P. Cechet (2000), The impact of the diurnal variation of albedo on the remote sensing of the daily mean albedo of grassland, *J. Appl. Meteorol.*, *39*, 231–244.

Jensen, E., D. Starr, and O. B. Toon (2004), Mission investigates tropical cirrus clouds, *Eos Trans. AGU*, *85*, 45–49.

Jin, Y., C. B. Schaaf, F. Gao, X. Li, and A. H. Strahler (2003), Consistency of MODIS surface bidirectional reflectance distribution function and albedo retrievals: 1. Algorithm performance, *J. Geophys. Res.*, *108*(D5), 4158, doi:10.1029/2002JD002803.

Keil, A., M. Wendisch, and E. Brügemann (2001), Measured profiles of aerosol particle absorption and its influence on clear-sky solar radiative forcing, *J. Geophys. Res.*, *106*, 1237–1247.

Kiehl, J. T., and K. E. Trenberth (1997), Earth's annual global mean energy budget, *Bull. Am. Meteorol. Soc.*, *78*, 197–208.

Kneizys, F. X., E. P. Shettle, L. W. Abreu, J. H. Chetwynd, G. P. Anderson, W. O. Gallery, J. E. A. Selby, and S. A. Clough (1988), Users guide to LOWTRAN-7, *AFGL-TR-88-0177*, Air Force Geophys. Lab., Bedford, Mass.

Li, Z., M. C. Cribb, and A. P. Trishchenko (2002), Impact of surface inhomogeneity on solar radiative transfer under overcast conditions, *J. Geophys. Res.*, *107*(D16), 4294, doi:10.1029/2001JD000976.

Michalsky, J., Q. Min, J. Barnard, R. Marchand, and P. Pilewskie (2003), Simultaneous spectral albedo measurements near the Atmospheric Radiation Measurement Southern Great Plains (ARM SGP) central facility, *J. Geophys. Res.*, *108*(D8), 4254, doi:10.1029/2002JD002906.

Nakajima, T., and M. Tanaka (1986), Matrix formulations for the transfer of solar radiation in a plane-parallel scattering atmosphere, *J. Quant. Spectrosc. Radiat. Transfer*, *35*, 13–21.

Nakajima, T., and M. Tanaka (1988), Algorithms for radiative intensity calculations in moderately thick atmospheres using a truncation approximation, *J. Quant. Spectrosc. Radiat. Transfer*, *40*, 51–69.

Ohlmann, J. C., D. A. Siegel, and C. D. Mobley (2000), Ocean radiant heating, part I: Optical influences, *J. Phys. Oceanogr.*, *30*, 1833–1848.

Pilewskie, P., J. Pommier, R. Bergstrom, W. Gore, S. Howard, M. Rabbette, B. Schmid, P. V. Hobbs, and S. C. Tsay (2003), Solar spectral radiative forcing during the Southern African Regional Science Initiative, *J. Geophys. Res.*, *108*(D13), 8486, doi:10.1029/2002JD002411.

Shettle, E. P. (1989), Models of aerosols, clouds and precipitation for atmospheric propagation studies, *AGARD Conf.*, *454*.

Stamnes, K., S. C. Tsay, W. Wiscombe, and K. Jayaweera (1988), A numerically stable algorithm for discrete-ordinate-method radiative transfer in multiple scattering and emitting layered media, *Appl. Opt.*, *27*, 2502–2509.

Webb, A. R., I. M. Stromberg, H. Li, and L. M. Bartlett (2000), Airborne spectral measurements of surface reflectivity at ultraviolet and visible wavelengths, *J. Geophys. Res.*, *105*, 4945–4948.

Wendisch, M. (2003), Absorption of solar radiation in the cloudless and cloudy atmosphere, Habilitation thesis, 174 pp., Wiss. Mitt. aus dem Inst. für Meteorol. der Univ. Leipzig, Leipzig, Germany.

Wendisch, M., and B. Mayer (2003), Vertical distribution of spectral solar irradiance in the cloudless sky-A case study, *Geophys. Res. Lett.*, *30*(4), 1183, doi:10.1029/2002GL016529.

Wendisch, M., D. Müller, D. Schell, and J. Heintzenberg (2001), An airborne spectral Albedometer with active horizontal stabilization, *J. Atmos. Oceanic Technol.*, *18*, 1856–1866.

Wendisch, M., et al. (2002), Aerosol-radiation interaction in the cloudless atmosphere during LACE 98: 1. Measured and calculated broadband solar and spectral surface insolations, *J. Geophys. Res.*, *107*(D21), 8124, doi:10.1029/2000JD000226.

H. Guan, S. Howard, and J. Pommier, Bay Area Environmental Research (BAER) Institute, 560 Third Street West, Sonoma, CA 95476, USA. (guan@clio.arc.nasa.gov; howard@solat.arc.nasa.gov; jpommier@mail.arc.nasa.gov)

E. Jäkel, S. Schmidt, and M. Wendisch, Leibniz-Institut für Troposphärenforschung (IfT), Permoserstraße. 15, D-04318 Leipzig, Germany. (jaekel@tropos.de; schmidt@tropos.de; wendisch@tropos.de)

H. H. Jonsson, Center for Interdisciplinary Remotely-Piloted Aircraft Studies (CIRPAS), 3240 Imjin Rd., Hangar #510, Marina, CA 93933, USA. (hjonsson@nps.navy.mil)

B. Mayer, Institut für Physik der Atmosphäre, Deutsches Zentrum für Luft- und Raumfahrt (DLR), Oberpfaffenhofen, D-82234 Wessling, Germany. (bernhard.mayer@dlr.de)

P. Pilewskie, NASA Ames Research Center, M/S 245-4 Moffett Field, CA 94035-1000, USA. (peter.pilewskie-1@nasa.gov)

M. Schröder, Institut für Weltraumwissenschaften, Freie Universität Berlin, Carl-Heinrich-Becker-Weg 6-10, D-12165 Berlin, Germany. (marc.schroeder@wew.fu-berlin.de)